Experimental and numerical evaluation of the compressive and shear behavior of unstabilized rammed earth

Fernando Ávila [ID] · **Mario Fagone** · **Rafael Gallego** · **Esther Puertas** · **Giovanna Ranocchiai**

Abstract Rammed earth has a longstanding tradition as a construction method and has recently gained renewed interest as an eco-friendly building technique. To employ it effectively in contemporary constructions, proper characterization of its mechanical properties and the development of predictive models become essential. Rammed earth structures usually work under compression, but their low shear strength makes this a key parameter for failure. Considering this, in the present study a mechanical characterization of rammed earth under compression and shear is carried out via laboratory tests, and the results are used to develop a numerical model (finite elements method) that can simulate rammed earth behavior under compressive and shear loads. The results show a good performance of the numerical models, accurately replicating the material behavior observed in laboratory. These numerical models are essential to predict the behavior and ensure an efficient and safe design of rammed earth structures.

Keywords Unstabilized rammed earth · Compressive strength · Shear strength · Mechanical characterization · FEM · Earthen construction

F. Ávila (✉) · R. Gallego · E. Puertas
Department of Structural Mechanics and Hydraulic Engineering, University of Granada, Av. Fuentenueva, Granada 18001, Spain
e-mail: favila@ugr.es

R. Gallego
e-mail: gallego@ugr.es

E. Puertas
e-mail: epuertas@ugr.es

M. Fagone · G. Ranocchiai
Department of Civil and Environmental Engineering, University of Florence, Via di S. Marta 3, Florence 50139, Italy
e-mail: mario.fagone@unifi.it

G. Ranocchiai
e-mail: giovanna.ranocchiai@unifi.it

1 Introduction

In an increasingly sustainability-conscious world, traditional construction techniques and environmentally friendly materials are gaining renewed interest from builders and researchers. One such example are the building techniques using raw earth as a primary construction material.

Earth has been used as a building material for thousands of years, with several and diverse construction techniques developed all over the world [1–3]. Even today, about 30 to 40% of the world population lives in houses built with earth [3–6]. The historical and current success of this kind of constructions is due to the availability of the material at low price and their mechanical and hygrothermal properties, together with a construction processes that do not require highly specialized labor [1, 7].

When earth is compacted in layers between temporary formwork, the construction method is called

rammed earth (RE). This technique is present in several countries, used both for small houses and for bigger structures such as fortress, palaces or city walls [1, 8–10]. The most traditional technique is the so-called unstabilized rammed earth (URE), which uses only water and soil, including a certain amount of clay that acts as the only binder for the mixture. In the last decades, the addition of stabilizers –mainly cement– to improve RE properties has been very common [11]. Also reinforcements based on natural and artificial fabrics have been investigated [12, 13]. However, the use of stabilizers increases the environmental impact of RE (e.g. RE stabilized with 8% cement implies more than 14 times the carbon emissions and 10 times the embodied energy than the same volume of RE without stabilizers) [11], so URE is again generating growing interest as a much more eco-friendly construction technique that can still offer a very good mechanical performance [14–17].

Structural safety of traditional RE construction was based on geometrical relationships and qualitative rules, but more accurate design bases are needed nowadays in order to meet the high requirements established by construction standards. With this aim, several studies have been developed over the last years regarding the mechanical characterization of RE. Also, some authors have proposed constitutive models to represent the mechanical behavior and failure mechanisms of the material. The research, however, has been mainly focused on the compressive behavior (RE is intended to work under compression) and has been developed mostly for stabilized rammed earth (SRE), in the pursuit of finding the material with the best mechanical performance [11].

Considering the relevance of URE as a historic construction technique and its huge potential as a modern eco-friendly building method, the present study aims to develop a numerical model of RE without stabilizers that accurately reproduces its behavior both under compression and shear. As complex behavioral models need a significant amount of input data, experimental tests were developed: unconfined compression tests (UCT) on cylindrical specimens to analyze the compressive behavior – this kind of tests have been frequently carried out for RE characterization by diverse authors –, and diagonal compression tests (DCT) on larger prismatic samples to define the shear behavior and fracture and failure mechanisms. Despite the fact that tensile and shear behavior is one of the most relevant parameters in the analysis of RE

failure (especially under extreme conditions) [18, 19], there are very few examples in literature regarding diagonal (shear) testing of RE [5, 6, 20].

In a second part of the study, a finite element model of the diagonal test was developed, defining an elastoplastic behavioral model for the material that included the mechanical properties obtained experimentally. Some other parameters that could not be assessed from the tests were obtained from literature, and then their influence was evaluated though a sensitivity analysis.

## 2 Experimental campaign

2.1 Materials

The natural soil used in the experimental campaign of the present study comes from Seggiano (Grosseto, Italy), and can be classified, according to the European Soil Classification System (ESCS, ISO 14688-2:2018), as well-graded sand, after been passed through an 8mm sieve in order to remove the coarser particles. The particle size distribution of the resulting earthen material – shown in Fig. 1 – contains 14% clay, 31% silt, 42% sand and 13% gravel, in agreement with several recommendations for URE source materials [14, 17, 21, 22]. The mineralogical composition of the soil is shown in Table 1; it was determined by X-ray diffractometer, and clay mineral analysis was successively performed interpreting the variations of lattice distances related to the basal reflections that occur following specific treatments [23].

The consistency limits, maximum dry density (MDD) and optimum moisture content (OMC) where also evaluated. The soil had a plastic limit equal to 18% and liquid limit equal to 38%, leading to a plastic index of 20, according to the methodology indicated in ASTM D4318 [24]. The standard Proctor test (method C) was performed according to ASTM D698 [25], obtaining a OMC of 13% corresponding to a MDD equal to 1.83g/cm^3. The geotechnical characteristics of the soil, together with its mineralogical composition, are summarized in Table 1.

2.2 Specimen manufacturing

Two different types of unstabilized rammed earth specimens were prepared for the experimental tests: small cylinders (diameter 10.1cm, height 11.5cm) for
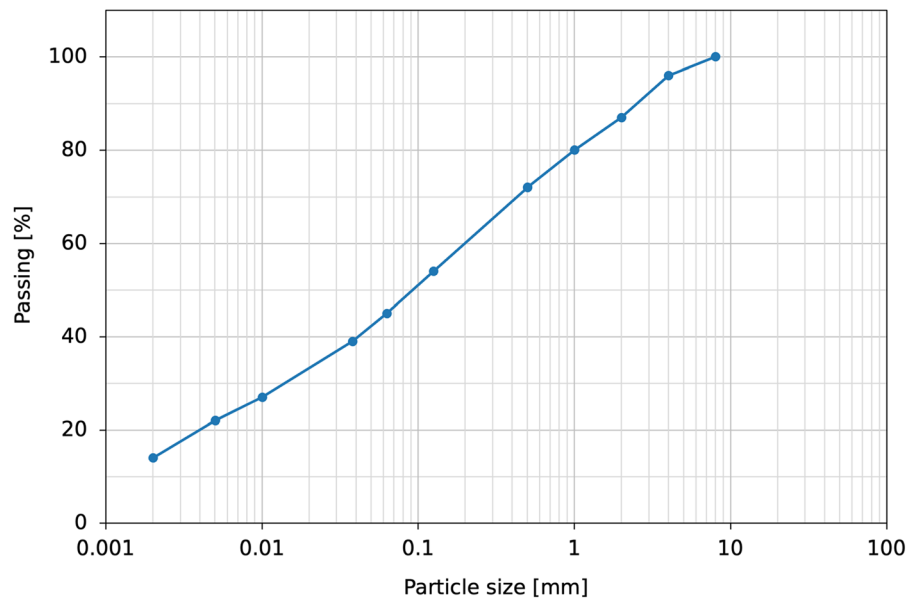
Fig. 1 Particle size distribution of the soil

Table 1 Main mineralogical and geotechnical characteristics of the soil

Mineralogical composition		Geotechnical properties	
Quartz	27%	Plastic limit	18%
Calcite	25%	Liquid limit	38%
Clay minerals	48%	Plastic index	20
	– Illite 40%	OMC	13%
	– Vermiculite 40%	MDD	1.83g/cm^3
	– Kaolinite 20%		

the uniaxial compression tests, and large panels (50 cm × 50 cm × 10 cm) for the diagonal compression tests. The dimensions of the cylindrical samples were chosen in order to be able to use the Proctor mold [26] to manufacture the samples, which ensures that the soil receives the targeted compaction energy and makes the manufacturing process easily replicable. This is particularly useful considering the great variety of testing methodologies currently present in RE literature [18]. It should be noted, however, that the slenderness of these samples is lower than the usual one used for compression tests on cylindrical concrete samples (i.e. 2.0), so it may generate some variations if the results are compared to that of other studies in the literature.

The prismatic samples are a scaled version of the specimens used in the standard test method for diagonal tension in masonry assemblages [27]. These reduced dimensions have already been successfully used in previous studies for the evaluation of the shear strength or RE materials [5, 28].

To prepare the specimens, the natural soil was uniformly mixed with 13% water, reaching the water content equal to the OMC of the soil, in agreement with the recommendations of Walker et al. [17] and standard NZS-4298 [29]. This mixture was then poured into the molds and compacted. A 10.1cm-diameter Proctor mold was used for the cylindrical specimens, compacting the soil in three uniform layers by dropping a standard Proctor rammer (2.50kg) 25 times per layer from a height of 30.5cm, subjecting the soil to a total compactive effort of about 600kN m/m^3 [25]. Although Proctor compaction tests do not apply the same energy as the one applied on a construction site, they are considered as a useful to assess the appropriate manufacturing water content for RE

(a)   (b)
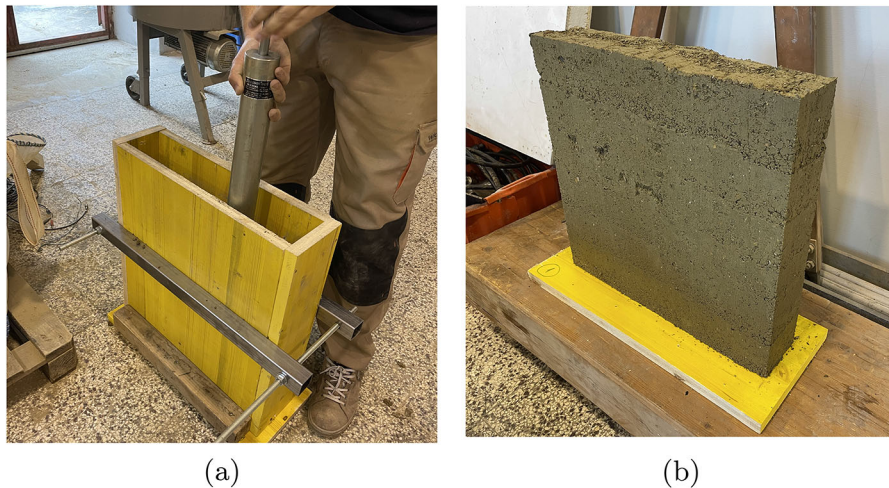
Fig. 2 Prismatic sample: compaction process (**a**) and manufactured specimen (**b**)

structures [17, 18, 30, 31]. According to previous studies [18, 32], results of standard Proctor tests could be more accurate when a manual rammer is used for the construction, while modified Proctor tests could fit better if pneumatic compaction is expected.

A wooden formwork was manufactured for the prismatic samples, externally reinforced with steel bars to avoid undesired deformations (Fig. 2). The soil was compacted in six ca. 8.33cm-thick layers using a modified Proctor test rammer [26] (4.54kg) dropped 123 times per layer from a height of 45.7cm, in order to reach the same compactive effort per unit volume. Just after the final layer was compacted, the samples were carefully removed from the mold and stored for curing under constant ambient conditions –about 25°C and 60% relative humidity– during 28 days. After 10 to 15 days of curing, the mass of the specimens reached a constant value. A total of four cylindrical samples (C1 to C4) and three panels (P1 to P3) were manufactured. The compaction process for each sample was completed within an hour after the water was added to the soil, to avoid significant moisture losses due to evaporation [33, 34].

2.3 Testing methodology

The experimental part of the present study includes the evaluation of the compressive and shear behavior of the URE samples, through uniaxial and diagonal compression tests, respectively. The UCT, in the absence of specific standards for RE materials, were performed according to ASTM D1633 "Standard Test Methods for Compressive Strength of Molded Soil-Cement Cylinders" [35], applying a homogeneously distributed load on the upper face of the cylindrical specimens, in the direction perpendicular to the earth layers. The surfaces in contact with the bearing blocks were leveled by means of a disc grinder. A displacement-controlled testing machine was used for the test, with loading speed equal to 1.3mm/min. A specimen subjected to UCT, after failure, is shown in Fig. 3a.

For the DCT, the indications of standard ASTM E519 "Standard Test Method for Diagonal Tension (Shear) in Masonry Assemblages" [27]. The load was applied on the top steel loading shoe, as a monotonic displacement at a rate of 1.2mm/min. The displacements along both main diagonals, in both faces, were measured by means of displacement transducers with gauge length 150mm. The setup for the DCT is shown in Fig. 3b.

2.4 Experimental results

From the uniaxial compression tests, the stress–strain curves were obtained (Fig. 4); calculating the stress as the ratio between the applied load and the cross area of the sample, and the strain as the ratio between the total vertical displacement and the initial height of the specimen (i.e. stroke of the test machine). It is possible to observe an initial linear branch, where the behavior of the material can be assumed elastic, followed by another linear branch with lower slope, where the

(a)　　　　　　　　　　　　　　　　(b)
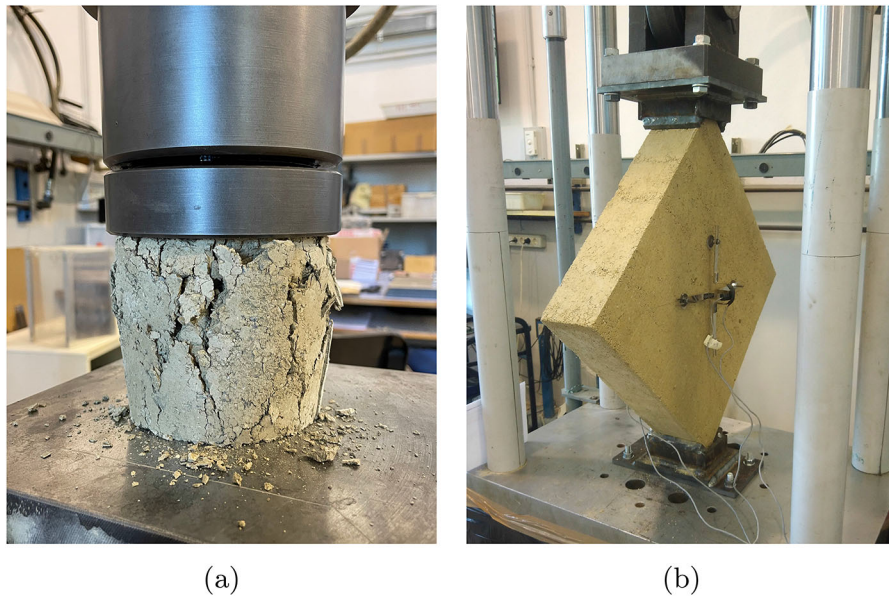
Fig. 3 Cylindrical specimen under UCT, after failure (**a**), and prismatic specimen under DCT, before failure (**b**)
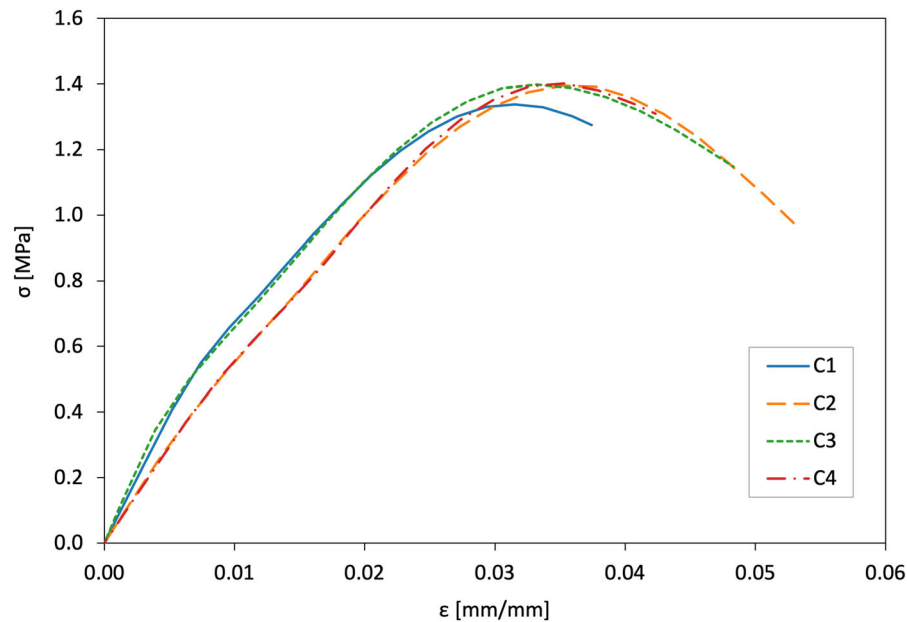
Fig. 4 Stress–strain curves from uniaxial compression tests

generation and propagation of microcracks becomes more significant. A non-linear behavior continues until reaching the peak strength, followed by a softening branch until failure.

Table 2 shows the main parameters obtained from the UCT. At the moment of testing, the specimens had an average water content equal to 3.9%. The unconfined compressive strength (UCS) obtained in the tests is within the range usually indicated in the existing literature about URE, between 1.00 and 2.00 MPa [18]. Similar compressive strengths have been obtained by several authors for RE without stabilizers using both cubic and cylindrical specimens [36–39]. Very small dispersion between the UCS results was

observed – coefficient of variation (CV) equal to 1.8% –, especially considering the intrinsic heterogeneity of material; which proves the effectiveness of the manufacturing and testing methodology followed in this study.

Diagonal compression tests were performed on three different prismatic specimens, loading them until failure, obtaining the cracking patterns represented in Fig. 5. Cracks started approximately at the center of the specimens and spread following a diagonal orientation towards the loading shoes. Crack propagation was also conditioned by the presence of the interfaces between the earth layers. Smaller cracks also appeared, before reaching the peak load, near the interfaces at border of the panels.

From the results of the DCT, the shear stress (S_S [MPa]) and shear strain (γ [mm/mm]) of the specimens were calculated, according to Eqs. 1 and 2, as defined in ASTM E519 [27]. The relationship between these two parameters along the test is represented in Fig. 6. The softening branch is shorter for sample D3 because one of the gauges moved after the peak load and so further displacements could not be properly measured.

$$S_s = \frac{0.707P}{A_n} \tag{1}$$

$$\gamma = \frac{\Delta x + \Delta y}{g} \tag{2}$$

where

- P is the applied load in N;
- A_n is the net area of the sample in mm^2;
- Δx and Δy are de displacements in the direction parallel and perpendicular to loading, respectively; and
- g is the gauge length.

The values obtained for these parameters in the DCT, together with the initial modulus of rigidity (G_0) – calculated as the initial slope of the shear stress–strain –, are shown in Table 3. The average water content in the samples at testing was equal to 5.8%. As it happened with the UCT, the dispersion in the results is very low for the strength and higher for the modulus of rigidity and the strain. The average S_s obtained in this study, is similar to the values found in literature [19, 39], although there are very few studies evaluating this parameter for URE. The shear strength of the material, according to the present study, is equal to 10% of the compressive strength. There are not relationships defined in literature between these two parameters, while the same relationship (1:10) has been found by several authors between the tensile and the compressive strength [19, 37, 39–41].

From the initial modulus of rigidity and Poisson's ratio (v) it is possible to estimate the elastic modulus of an isotropic material as $E = 2G(1 + v)$. As some relevant studies have already pointed [19], although it
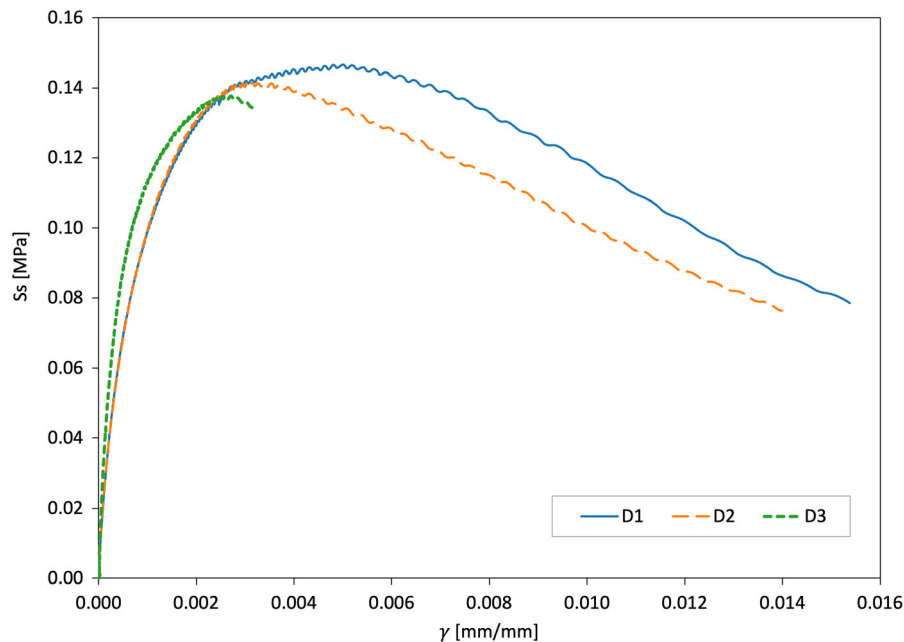
Table 2 Results from UCT on URE cylindrical specimens

Sample	ρ_{test} [g/cm^3]	UCS (MPa) [MPa]	ε_{ucs} [m/m]
C1	1.94	1.36	0.031
C2	1.94	1.41	0.036
C3	1.95	1.41	0.034
C4	1.96	1.41	0.036
Mean	1.94	1.40	0.034
CV	2.3%	1.8%	6.8%

ρ_{test}: density at testing; UCS: unconfined compressive strength; ε_{ucs}: strain at maximum strength
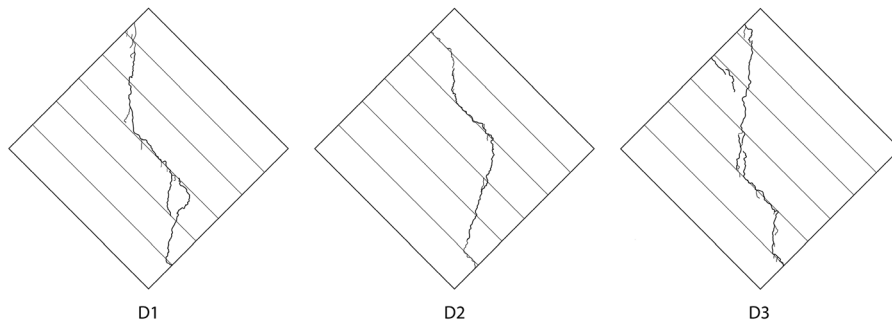
Fig. 5 Cracking patterns at failure of the URE panels in DCT

Fig. 6 Shear stress–strain curves from diagonal compression tests

Table 3 Results from DCT on URE panels

Sample	ρ_{test} (g/cm^3)	S_s (MPa)	G_0 (MPa)	γ_{ss} (mm/m)
D1	1.90	0.15	236.5	4.92
D2	1.93	0.14	251.3	2.93
D3	1.92	0.14	288.2	2.82
Mean	1.92	0.14	258.6	3.56
CV	1.1%	3.2%	10.3%	33.2%

ρ_{test}: density at testing; S_s: shear strength; G_0: initial modulus of rigidity; γ_{ss}: shear strain at maximum strength

might be surprising, the assumption of an isotropic material is totally acceptable for RE. Therefore, considering a value of the Poisson's ratio equal to 0.27 [18, 39, 40, 42], an elastic modulus of 655MPa is obtained. Values of the Poisson's ratio of URE in literature are generally between 0.22 and 0.30 [18]; 0.27 can be considered as a value of consensus frequently used by diverse authors in previous studies [39, 40, 42–44].

The value of the elastic modulus equal to 655MPa is within the range usually found in URE literature, frequently between 350 and 1 000MPa [1, 6, 30, 37, 39, 45–47]. The E/f_c ratio obtained, equal to ca. 470, is also similar to those shown in other existing studies about URE [37, 43, 48]. The E value obtained from the DCT is considerably higher than the one measured in the UCT, equal to ca. 80MPa (CV = 22%). In fact, it has been observed that measuring the deformations directly from the displacements of the testing machine – as it was done in the UCT – significantly underestimates the stiffness of the earthen material, as the settling of the soil particles at the contact surface with the supports results in greater deformations [49, 50]. It should be noted, in addition, that the enormous variability in the measurement techniques, the differences in preparation protocols for the specimens and the dispersion in the results existing in literature does not allow to define a value of consensus for the stiffness of RE.

3 Numerical analysis

A numerical simulation of the diagonal compression test was carried out through finite element method (FEM). The material is modeled as continuum and homogeneous – without taking into account the existence of layers or the interaction between them –, an approach frequently used for RE, as it allows to obtain accurate results using models with lower complexity [42, 44, 51]. The numerical analysis

described in the present study was carried out using FEM software Abaqus v.2022 [52].

3.1 Constitutive law

The continuum, plasticity-based, damage model "concrete damage plasticity" (CDP), implemented in Abaqus, was used to describe the behavior of the material. CDP is based on the constitutive model proposed by Lubliner et al. [53], with the modifications introduced by Lee and Fenves [54]. Although it was initially designed for concrete, its characteristics – such as the different yield strengths in tension and compression and the fact that it assumes that the main two failure mechanisms are tensile cracking and compressive crushing of the material – make it particularly suitable for advanced macroscopic modeling of brittle and quasi-brittle materials [22, 55, 56]. The uniaxial stress–strain relations used in the CDP model are shown in Fig. 7.

This behavioral model uses a Drucker-Prager surface as multidimensional strength domain, which can be modified by a factor K_c (ratio of the second stress invariant on the tensile meridian), that allows to deform the failure surface, with $K_c = 1$ meaning a circular yield surface in the deviatoric plane. Other parameters defining the CDP model are the flow potential eccentricity (ϵ), representing the rate at which the flow potential function approaches the asymptote (when the eccentricity tends to zero the function tends to a straight line); the biaxial strength ratio (σ_{b0}/σ_{c0}); the viscosity parameter (μ); and the

dilation angle (φ). The values of these parameters considered in the present study are shown in Table 4 and were defined following the recommendations present in literature for RE modeling [22, 55, 56] and in Abaqus documentation [57]. For the dilation angle, it was analyzed that varying its value from 0° to 20° had a negligible effect on the stress–strain behavior of the material.

Together with these general parameters, Abaqus' CDP model requires the definition of the elastic properties of the material and the inelastic compressive and tensile behavior. For the RE material analyzed in the present study, an elastic modulus of 655 MPa—obtained from the experimental DCT— was considered, with a Poisson's ratio assumed equal to 0.27, according to literature, as previously indicated.

For the compressive behavior, the inelastic stress–strain data obtained in UCT was introduced. The tensile behavior of the material was defined by specifying the fracture energy and the tensile strength, assuming a linear loss of strength after cracking [58, 59]. The value of these parameters were assessed through a sensitivity test on the model.

3.2 Finite elements model

The FEM model for the DCT comprised three parts: a 50 cm × 50 cm × 10 cm prism with CDP behavioral model—as described in the previous section—representing the URE sample, and two L-shaped loading shoes defined as rigid solids. The contact surface
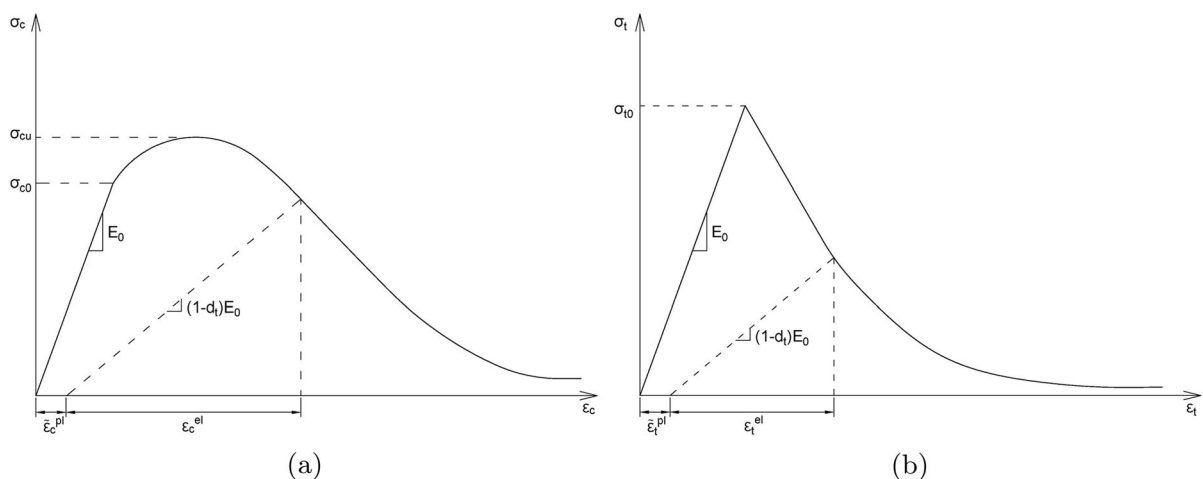
Fig. 7 Stress–strain curves in the CDP model under uniaxial loading in compression (a) and tension (b) [57]

Table 4 Parameters used in the CDP model

Parameter	Value
K_c	2/3
ϵ	0.1
σ_{b0}/σ_{c0}	1.16
μ	0.001
φ	10°

Fig. 8 Finite elements model for diagonal compression test
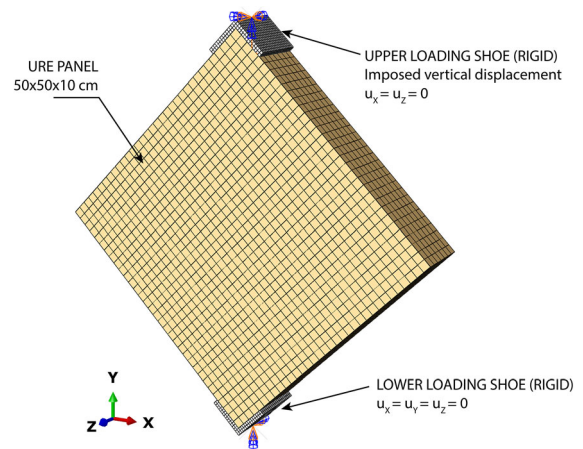
between the loading shoes and the panel was defined with a "hard" contact normal behavior plus a penalty (friction) tangential behavior [60], with friction coefficient equal to 0.2. A sensitivity analysis was carried out for this friction coefficient, observing that changes near to the chosen value of 0.2 had a negligible effect on the general behavior of the model, while much higher values produced an abnormal behavior in the zone near the shoe-sample contact. The loading shoes had all displacements constrained but the vertical displacement of the top shoe; this displacement was monotonically incremented up to a value of 5.0mm, so that the significant region of the load–displacement equilibrium path was covered. Eight-node linear brick elements were used, and a static analysis was performed.

Figure 8 shows the geometry of the finite element model for the DCT in Abaqus.

3.3 Calibration and results

The model was evaluated varying the two parameters that describe the tensile behavior of the CDP material model (i.e. tensile strength and fracture energy) in order to assess their effect. For the tensile strength, according to the results in literature, values between 0.14 MPa (10% of the UCS) and 0.17 MPa were assumed [6, 37, 39–41]. For the fracture energy, there is not much information in URE literature, but some authors show results between 10 and 20 N/m [40, 45, 61]; while Abaqus recommends using typical values from 40 to 120 N/m [57] (as the model is originally designed for concrete). Considering this, the model was analyzed for fracture energy values equal to 10, 20, 30 and 40 N/m. The results (shear strength-stress curves) obtained simulating the DCT for all the possible combinations of these two parameters are shown in Fig. 9.

It can be observed that the first part of the $S_s - \gamma$ curve, corresponding to the elastoplastic branch for increasing load, fits very well with the experimental results and does not vary when modifying the tensile parameters of the model, as the material here is mostly under compression. Before reaching the maximum load, when the behavior becomes more plastic and tension-dependent, the shape of the curves highly depends on the G_f and f_t values. Increasing the fracture energy increases the peak shear strength and the corresponding shear stress. Also, high G_f values lead to a smooth softening branch, while low values cause a fast decrease of the stress after the peak load. The tensile strength, on the other hand, does not significantly affect the post-peak behavior, but increases the maximum shear stress reached. The shear strain at which this stress is reached is also increased but not that much.

According to these results, a fracture energy in the CDP model of at least 20 N/m is required to reach the experimental peak stress, and $G_f = 40$ N/m is needed to properly represent the post-peak behavior. At the same time, tensile strengths between 0.15 and 0.16MPa were able to provide a good adjustment of the curve at the peak strength and for the values around this maximum. With these G_f and f_t values, the model reached a maximum shear stress of ca. 0.14 MPa at a shear strain between 3.2 and 4.0 mm/m, very close to the values obtained in the laboratory tests. Also the rest of the $S_s - \gamma$ curves show a behavior similar to the one observed experimentally.

The failure mode obtained with the FEA was evaluated and compared with the one observed experimentally. The "tensile equivalent plastic strain"
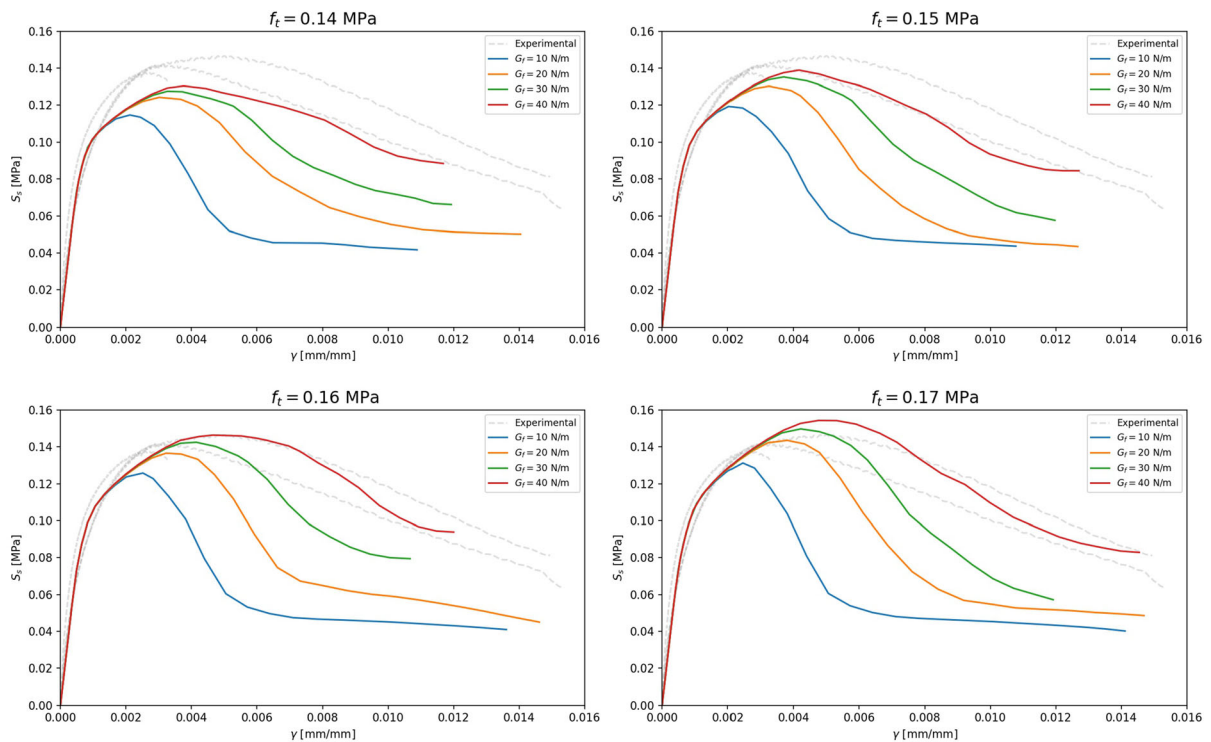
Fig. 9 Shear stress–strain curves obtained in the FEA with varying fracture energy (G_f) and tensile strength (f_t)

(PEEQT in Abaqus) is a useful variable to evaluate the damage in a brittle material [57, 62]. In fact, it can be assumed that cracking initiates at points where the tensile equivalent plastic strain and the maximum principal plastic strain are greater than zero [53]. These two parameters are shown in Fig. 10, where it can be observed that the damage in the model concentrates in central part of the sample, subjected to strong tensile stresses, and in the stress concentration zone in the contact between the URE specimen and the supports. These are the zones were the cracks were developed in the laboratory tests. This correspondence between the stresses obtained in the model and the failure in the real sample is also observed when superimposing the maximum (tensile) principal stress and the cracks obtained in the tested URE samples, as shown in Fig. 11.

4 Conclusions

Understanding the mechanical behavior of unstabilized rammed earth is essential in order to introduce this environmentally sustainable building technique in new constructions, and also to properly preserve the abundant architectural heritage built with this material. In the present study, the compressive and shear behavior of URE were evaluated through unconfined compression tests and diagonal compression tests, and the results were used to develop a finite element model of the latter.

From the experimental tests, an average compressive strength of 1.4MPa was obtained, similar to values frequently shown in literature for URE. A manufacturing methodology including the use of a standardized Proctor mold and the control of the compaction energy allowed to obtain a very small dispersion in the results (e.g. coefficient of variation of 1.8% for the compressive strength), which is particularly relevant considering the high heterogeneity frequently shown by rammed earth. It should be noted, however, that these results were obtained on a limited number of samples of a certain soil type with a particular manufacturing water content and compaction energy, and should be taken with caution before extrapolation to on-site construction conditions.
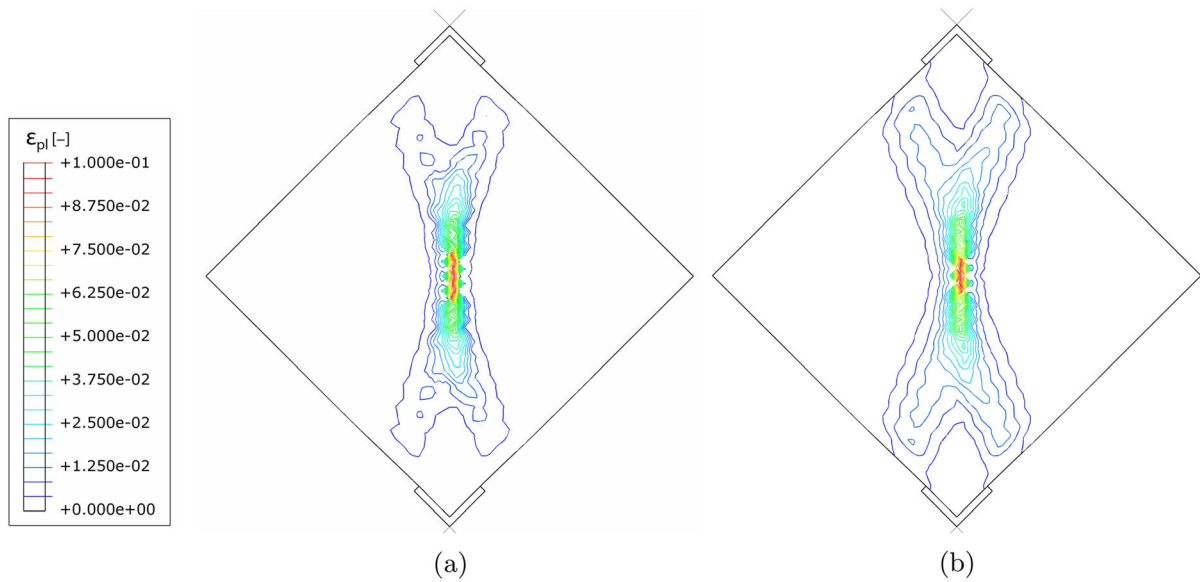
Fig. 10 Isolines of tensile equivalent plastic strain (**a**) and maximum (tensile) principal plastic strain (**b**) from FEA of DCT
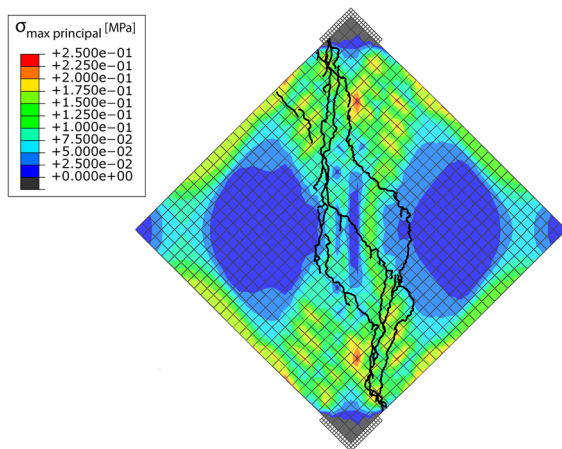
Fig. 11 Maximum (tensile) principal stress at the end of FEM test (shear strain 0.01m/m), and cracks from experimental tests. FE model with $G_f = 30$N/m and $f_t = 0,16$MPa

The shear strength of the material, obtained from the DCT following the procedure indicated by the ASTM for masonry assemblages, was equal to 0.14MPa, 10% of the compressive strength. This relationship has been observed by previous authors between the compressive and the tensile strength of rammed earth. In this experiments it was also possible to observe the crack development process, following a diagonal from one support to the other, and also influenced by the interfaces between the earth layers.

In the second part of the study, the FEM model developed with the software Abaqus using the experimental data, was proved to be useful for simulating the behavior of the RE material. Concrete damage plasticity was used as the behavioral model. The experimental data was enough to define the compressive behavior of the material, but to simulate the diagonal compression test it was also necessary to define the tensile strength and fracture energy as input parameters. The sensitivity analysis performed showed that minimum fracture energy of 20N/m was needed to reach the experimental peak stress, with tensile strengths between 0.15 and 0.16 MPa. The post-peak behavior was more accurately simulated with higher fracture energy values (30–40 N/m), although they are slightly higher than the experimental values usually obtained for earthen materials.

The numerical analysis of the diagonal tests also showed a stress distribution coherent with the experimental results and the crack propagation paths that lead to the failure of the specimen. Shear behavior is particularly relevant in the failure mechanisms of rammed earth structures under extreme loads – such as a seismic event –, so the results of this study can be used in a further step of the investigation to assess structural vulnerability of rammed earth constructions and ensure their integrity.

Regarding the limitations of the present study, it should be taken into account that the results were

obtained on a limited number of samples, using a certain soil type with a particular water content (standard Proctor optimum moisture content), and providing a specific compaction energy (standard Proctor compaction energy). These results may vary for different soil types and/or compaction and manufacturing protocols; further experiments and developments would be relevant considering the potential variability of earthen resources and test conditions.

Declarations

References

1. Minke G (2006) Building with earth: design and technology of a sustainable architecture. Birkhäuser - Publishers for Architecture, Basel

2. Mohammad R (2012) Foreword. In: Eloundou L, Joffroy T (eds) Earthen archit. Today's World Proc. UNESCO Int. Colloq. Conserv. World Herit. Earthen Archit., p 7. UNESCO, CRAterre, Paris, France. http://whc.unesco.org/en/series/36/

3. Niroumand H, Zain MFM, Jamil M (2013) Various types of earth buildings. Proc Soc Behav Sci 89:226–230. https://doi.org/10.1016/j.sbspro.2013.08.839

4. Martínez Escobar D (2013) Earth architecure: building with rammed earth in a cold climate. Masther thesis, Chalmers University of Technology, Gothenburg, Sweden. http://libris.kb.se/bib/14702698?vw=short

5. Miccoli L, Müller U, Fontana P (2014) Mechanical behaviour of earthen materials: a comparison between earth block masonry, rammed earth and cob. Constr Build Mater 61:327–339. https://doi.org/10.1016/j.conbuildmat.2014.03.009

6. Yamin LE, Phillips CA, Reyes JC, Ruiz DM (2004) Seismic behavior and rehabilitation alternatives for adobe and rammed earth buildings. In: 13th world conference earthquake engineering (2942)

7. Maniatidis V, Walker P (2003) A review of rammed earth construction. Dev. rammed earth UK Hous. (May), 109

8. Martín-del-Rio JJ, Canivell J, Torres-González M, Mascort-Albea EJ, Romero-Hernández R, Alducin-Ochoa JM, Alejandre-Sánchez FJ (2021) Analysis of the materials and state of conservation of the medieval rammed earth walls of Seville (Spain). J Build Eng 44:103381. https://doi.org/10.1016/j.jobe.2021.103381

9. Gandreau D, Delboy L (2012) CRATerre-ENSAG (France): UNESCO World Heritage Inventory of Earthen Architecture, https://unesdoc.unesco.org/ark:/48223/pf0000217020

10. Vyncke J, Kupers L, Denies N (2018) Earth as building material: an overview of RILEM activities and recent innovations in geotechnics. MATEC web conference vol 149, 02001. https://doi.org/10.1051/matecconf/201714902001

11. Ávila F, Puertas E, Gallego R (2022) Characterization of the mechanical and physical properties of stabilized rammed earth: a review. Constr Build Mater 325:126693. https://doi.org/10.1016/j.conbuildmat.2022.126693

12. Fagone M, Loccarini F, Ranocchiai G (2017) Strength evaluation of jute fabric for the reinforcement of rammed earth structures. Compos Part B Eng 113:1–13. https://doi.org/10.1016/j.compositesb.2016.12.054

13. Fagone M, Kloft H, Loccarini F, Ranocchiai G (2019) Jute fabric as a reinforcement for rammed earth structures. Compos Part B Eng 175:107064. https://doi.org/10.1016/j.compositesb.2019.107064

14. Bui QB, Morel JC (2009) Assessing the anisotropy of rammed earth. Constr Build Mater 23(9):3005–3011. https://doi.org/10.1016/j.conbuildmat.2009.04.011

15. Morel J-C, Charef R, Hamard E, Fabbri A, Beckett C, Bui Q-B (2021) Earth as construction material in the circular economy context: practitioner perspectives on barriers to overcome. Philos. Trans. R. Soc. B Biol. Sci. **376**(1834), 20200182. https://doi.org/10.1098/rstb.2020.0182

16. Raavi SSD, Tripura DD (2020) Predicting and evaluating the engineering properties of unstabilized and cement stabilized fibre reinforced rammed earth blocks. Constr Build

Mater 262:120845. https://doi.org/10.1016/j.conbuildmat.2020.120845

17. Walker P, Keable R, Martin J, Maniatidis V (2005) Rammed earth: design and construction guidelines

18. Ávila F, Puertas E, Gallego R (2021) Characterization of the mechanical and physical properties of unstabilized rammed earth: a review. Constr Build Mater 270:121435. https://doi.org/10.1016/j.conbuildmat.2020.121435

19. Bui TT, Bui QB, Limam A, Maximilien S (2014) Failure of rammed earth walls: from observations to quantifications. Constr Build Mater 51:295–302. https://doi.org/10.1016/j.conbuildmat.2013.10.053

20. Pavan GS, Ullas SN, Nanjunda Rao KS (2020) Shear behavior of cement stabilized rammed earth assemblages. J. Build. Eng. 27:100966. https://doi.org/10.1016/j.jobe.2019.100966

21. Corbin A, Augarde C (2015) Investigation into the shear behaviour of rammed earth using shear box tests. In: First international conference bio-based build. mater., Clermont-Ferrand, France, pp 93–98

22. Loccarini F, Ranocchiai G, Rotunno T, Fagone M (2020) Experimental and numerical analyses of strengthened rammed earth masonry arches. Comput Struct 239:106329. https://doi.org/10.1016/j.compstruc.2020.106329

23. Banchellil A, Fratini F, Germanil M, Malesanil P, Manganelli Del Fà C (1997) The sandstones of the Florentine historic buildings: individuation of the marker and determination of the supply quarries of the rocks used in some Florentine monuments. Sci Technol Cult Herit 6(1):13–22

24. ASTM: D4318-17 Standard Test Methods for Liquid Limit, Plastic Limit, and Plasticity Index of Soils (2017). https://doi.org/10.1520/D4318-17E01.

25. ASTM: D698-12 Standard Test Methods for Laboratory Compaction Characteristics of Soil Using Standard Effort (12,400 ft-lbf/ft3 (600 kN-m/m3)) (2012). https://doi.org/10.1520/D0698-12E01.1

26. ASTM: D1557-12 Standard Test Methods for Laboratory Compaction Characteristics of Soil Using (2012). https://doi.org/10.1520/D1557-12.1

27. ASTM: E519/E519M-15 Standard Test Method for Diagonal Tension (Shear) in Masonry Assemblages (2015). https://doi.org/10.1520/E0519

28. Silva RA, Oliveira DV, Miranda T, Cristelo N, Escobar MC, Soares E (2013) Rammed earth construction with granitic residual soils: the case study of northern Portugal. Constr Build Mater 47:181–191. https://doi.org/10.1016/j.conbuildmat.2013.05.047

29. New Zealand Standard: NZS 4298:1998. Materials and workmanship for earth buildings (1998). https://www.standards.govt.nz/sponsored-standards/building-standards/nzs4298/

30. El Nabouch R (2017) Mechanical behavior of rammed earth walls under Pushover tests. Ph.d. thesis, Université Grenoble Alpes . https://tel.archives-ouvertes.fr/tel-01707009/document

31. Mesbah A, Morel JC, Olivier M (1999) Clayey soil behaviour under static compaction test. Mater Struct 32(223):687–694

32. Keable J (1996) Rammed earth structures. A code of practice. Intermediate Technology, London

33. Ciancio D, Beckett CTS, Carraro JAH (2014) Optimum lime content identification for lime-stabilised rammed earth. Constr Build Mater 53:59–65. https://doi.org/10.1016/j.conbuildmat.2013.11.077

34. Da Rocha CG, Consoli NC, Dalla Rosa Johann A (2014) Greening stabilized rammed earth: devising more sustainable dosages based on strength controlling equations. J Clean Prod 66:19–26. https://doi.org/10.1016/j.jclepro.2013.11.041

35. ASTM: D1633-17 Standard Test Methods for Compressive Strength of Molded Soil-Cement Cylinders (2017). https://doi.org/10.1520/D1633-00R07.combine

36. Arrigoni A, Pelosato R, Dotelli G, Beckett CTS, Ciancio D (2017) Weathering's beneficial effect on waste-stabilised rammed earth: a chemical and microstructural investigation. Constr Build Mater 140:157–166. https://doi.org/10.1016/j.conbuildmat.2017.02.009

37. Bui T, Bui QB, Limam A, Morel JC (2016) Modeling rammed earth wall using discrete element method. Contin Mech Thermodyn 28:523–538. https://doi.org/10.1007/s00161-015-0460-3

38. Pakand M, Toufigh V (2017) A multi-criteria study on rammed earth for low carbon buildings using a novel ANP-GA approach. Energy Build. 150:466–476. https://doi.org/10.1016/j.enbuild.2017.06.004

39. Silva RA, Oliveira DV, Schueremans L, Lourenço PB, Miranda T (2014) Modelling the structural behaviour of rammed earth components. Civil-Comp Proc. https://doi.org/10.4203/ccp.106.112

40. Miccoli L, Oliveira DV, Silva RA, Müller U, Schueremans L (2015) Static behaviour of rammed earth: experimental testing and finite element modelling. Mater Struct Constr 48(10):3443–3456. https://doi.org/10.1617/s11527-014-0411-7

41. Toufigh V, Kianfar E (2019) The effects of stabilizers on the thermal and the mechanical properties of rammed earth at various humidities and their environmental impacts. Constr Build Mater 200:616–629. https://doi.org/10.1016/j.conbuildmat.2018.12.050

42. Allahvirdizadeh R, Oliveira DV, Silva RA (2019) Numerical modeling of the seismic out-of-plane response of a plain and TRM-strengthened rammed earth subassembly. Eng Struct 193:43–56. https://doi.org/10.1016/j.engstruct.2019.05.022

43. El Nabouch R, Bui QB, Plé O, Perrotin P (2017) Assessing the in-plane seismic performance of rammed earth walls by using horizontal loading tests. Eng Struct 145:153–161. https://doi.org/10.1016/j.engstruct.2017.05.027

44. Silva RA, Oliveira DV, Miccoli L, Schueremans L (2014) Modelling of rammed earth under shear loading. In: SAHC2014–9th international conference analysis of historical construction, pp 14–17

45. Bui QB, Bui TT, Tran MP, Bui TL, Le HA (2019) Assessing the seismic behavior of Rammed earth walls with an L-Form cross-section. Sustain. https://doi.org/10.3390/su11051296

46. Röhlen U, Ziegert C (2011) Earth building practice. Planning–design–building. Bauwerk, Berlin, Germany

47. Tripura DD, Singh KD (2015) Characteristic properties of cement-stabilized rammed earth blocks. J Mater Civ Eng

27(7):04014214. https://doi.org/10.1061/(ASCE)MT.1943-5533.0001170

48. Bui QB, Morel JC, Hans S, Meunier N (2009) Compression behaviour of non-industrial materials in civil engineering by three scale experiments: The case of rammed earth. Mater Struct 42(8):1101–1116. https://doi.org/10.1617/s11527-008-9446-y

49. Koutous A, Hilali E (2023) Compression stress-strain curve of rammed earth: measuring and modelling. Results Eng. 18:101012. https://doi.org/10.1016/j.rineng.2023.101012

50. Misseri G, Rovero L (2022) Rammed earth as bi-modulus material: experimental and analytical investigations through Euler–Bernoulli and Timoshenko beam models. Int. J. Mason. Res. Innov. 7(5):482. https://doi.org/10.1504/IJMRI.2022.125359

51. Nowamooz H, Chazallon C (2011) Finite element modelling of a rammed earth wall. Constr Build Mater 25(4):2112–2121. https://doi.org/10.1016/j.conbuildmat.2010.11.021

52. Dassault Systèmes: Abaqus Unified FEA: Abaqus overview (2022). https://www.3ds.com/products-services/simulia/products/abaqus/

53. Lubliner J, Oliver J, Oller S, Oñate E (1989) A plastic-damage model for concrete. Int J Solids Struct 25(3):299–326. https://doi.org/10.1016/0020-7683(89)90050-4

54. Lee J, Fenves GL (1998) Plastic-damage model for cyclic loading of concrete structures. J Eng Mech 124(8):892–900. https://doi.org/10.1061/(ASCE)0733-9399(1998)124:8(892)

55. Bui TL, Bui TT, Bui QB, Nguyen XH, Limam A (2020) Out-of-plane behavior of rammed earth walls under seismic loading: finite element simulation. Structures 24:191–208. https://doi.org/10.1016/j.istruc.2020.01.009

56. Fagone M, Loccarini F, Ranocchiai G, Rotunno T (2019) Numerical constitutive models of low tensile strength materials for the description of mechanical behavior of rammed earth masonry. Key Eng Mater 817:30–36. https://doi.org/10.4028/www.scientific.net/KEM.817.30

57. Dassault Systèmes: 23.6.3 Concrete damaged plasticity. In: Abaqus Anal. User's Guid., (2013). http://130.149.89.49:2080/v6.13/books/usb/default.htm?startat=pt05ch23s06abm39.html

58. Arto I, Gallego R, Cifuentes H, Puertas E, Gutiérrez-Carrillo ML (2021) Fracture behavior of rammed earth in historic buildings. Constr Build Mater 289:123167. https://doi.org/10.1016/j.conbuildmat.2021.123167

59. Lenci S, Clementi F, Sadowski T (2012) Experimental determination of the fracture properties of unfired dry earth. Eng Fract Mech 87:62–72. https://doi.org/10.1016/j.engfracmech.2012.03.005

60. Dassault Systèmes: 37.2.3 Contact constraint enforcement methods in Abaqus/Explicit. In: Abaqus Anal. User's Man., (2012)

61. Sajad Hussaini SM, Toufigh V (2019) Strength and fracture behavior of rammed-earth materials. J Mater Civ Eng 31(10):1–13. https://doi.org/10.1061/(ASCE)MT.1943-5533.0002876

62. Ávila F, Puertas E, Gallego R (2020) Probabilistic reliability assessment of existing masonry buildings: the church of San Justo y Pastor. Eng Struct 223:111160. https://doi.org/10.1016/j.engstruct.2020.111160